

Synthesis and Characterization of the Mixed-Linker Copper(II) Coordination Polymer $[\text{Cu}(\text{HO}_3\text{PC}_6\text{H}_4\text{SO}_3)(\text{C}_{10}\text{H}_8\text{N}_2)] \cdot \text{H}_2\text{O}$

Palanikumar Maniam^[a] and Norbert Stock^{*[a]}

Dedicated to Professor Hanskarl Müller-Buschbaum on the Occasion of His 80th Birthday

Keywords: High-throughput screening; Copper; Coordination polymers; Phosphonato-sulfonates; X-ray diffraction

Abstract. A new copper(II) phosphonatobenzenesulfonate incorporating 4,4'-bipyridine (4,4'-*bipy*) as auxiliary ligand has been discovered through systematic high-throughput (HT) screening of the system $\text{Cu}(\text{NO}_3)_2 \cdot 3\text{H}_2\text{O}/\text{H}_2\text{O}_3\text{PC}_6\text{H}_4\text{SO}_3\text{H}/4,4'\text{-bipy}$ using different solvents. The hydrothermal synthesis of $[\text{Cu}(\text{HO}_3\text{PC}_6\text{H}_4\text{SO}_3)(\text{C}_{10}\text{H}_8\text{N}_2)] \cdot \text{H}_2\text{O}$ (**1**) was further optimized by screening various copper(II) salts. The crystal structure of **1** was determined by single-crystal X-ray diffraction and unveiled the presence of isolated sixfold coordinated Jahn–Teller-distorted Cu^{2+} ions. The isolated CuN_2O_4 octahedra are interconnected by phosphonate and sulfonate groups to form chains along the *c*-axis. The organic groups, namely phenyl rings and 4,4'-*bipy* molecules cross-link the chains into a three-dimensional framework. Water

molecules are found in the narrow voids in the structure which are held by weak hydrogen bonds. Upon dehydration, the structure of **1** undergoes a phase transition, which was confirmed by TG measurements and temperature dependent X-ray powder diffraction. The new structure of **1-h** was refined with Rietveld methods. Detailed inspection of the structure revealed the directional switching of the Jahn–Teller distortion upon de/rehydration. Weak ferro-/ferrimagnetic interactions were observed by magnetic investigations of **1**, which switch to antiferromagnetic below 3.5 K. Compounds **1** and **1-h** are further characterized by thermogravimetric and elemental analysis as well as IR spectroscopy.

Introduction

The field of inorganic-organic hybrid compounds encompasses many types of materials; i.e. amorphous nanocomposites, such as self-assembled mesoporous materials, to crystalline products.^[1] One intensively studied class of these compounds is coordination polymers.^[2,3] The organic building units that are mostly deployed in these materials are based on carboxylates ($R\text{-CO}_2^-$) and amines.^[4–7] On the other hand, sulfonate ($R\text{-SO}_3^-$) and phosphonate ($R\text{-PO}_3^{2-}$) based compounds have been less intensively investigated.^[8–11] The restriction of structural diversity with these functional groups compared to the -CO_2^- counterpart is mostly caused by the more flexible coordination modes as well as the higher number of coordinating atoms. Therefore, in general dense materials are formed.^[12,13] We are interested in the utilization of organic linker molecules containing two or more different functional groups for the synthesis of inorganic-organic hybrid compounds. In addition to the number of functional groups, their structure, coordination modes, as well as charge and acidity have a strong effect on the final crystal structure formation.

Examples from our previous work comprise the use of linkers containing phosphonate and carboxylate groups,^[14,15] phosphonate and amine groups such as imino-bis(methylphosphonate) units^[16] or imino-bis(methylphosphonate) and carboxylate units.^[17,18] Linkers containing phosphonic and sulfonic acid groups have only been recently investigated. By using the flexible linkers 2-phosphonoethane- and 4-phosphonobutane-sulfonic acid, our group has explored the synthesis of several hybrid compounds with different ions such as Cu^{2+} ,^[19,20] Sr^{2+} ,^[21] Ba^{2+} ,^[22] and lanthanide ions.^[23–25] Rigid phosphonoarylsulfonic acids, i.e. 3-phosphonobenzenesulfonic acid were employed by the group of Mao,^[26–30] 5-phosphono-1,3-disulfonic acid and 4-fluoro-3-sulfobenzylphosphonic acid by the group of Montoneri,^[31,32] mostly in combination with amine linkers.

The synthesis of most metal phosphonates is accomplished under hydrothermal conditions. Such reactions are often known to be strongly dependent on the process parameters, e.g. reaction time, temperature, heating rate, and the compositional parameters, e.g. molar composition of the starting materials, pH of the reaction mixture or overall concentration. An elegant way for the exploration of these complex systems can be carried out using high-throughput (HT) methods.^[33–35] These allow a systematic and efficient investigation of large parameter spaces giving rise to the accelerated discovery of new compounds and optimization of synthesis parameters. Due to the large amounts of data, reaction and structural trends can be derived. Our recent work on 4-phosphonobenzenesulfonic acid (H_3L) with HT methods has highlighted the discovery of sev-

* Prof. Dr. N. Stock
E-Mail: stock@ac.uni-kiel.de

[a] Institut für Anorganische Chemie,
Christian-Albrechts-Universität,
Max-Eyth-Strasse 2
24118 Kiel, Germany

Supporting information for this article is available on the WWW under <http://dx.doi.org/10.1002/zaac.201100202> or from the author.

eral compounds incorporating this linker and Cu^{2+} ions.^[36] Various CuO clusters ranging from mononuclear CuO_6 , binuclear Cu_2O_8 , hexanuclear Cu_6O_{24} to infinite chains of edge-sharing $\text{CuO}_5/\text{CuO}_6$ were observed in these phosphonosulfonate compounds. We concentrated on the usage of copper(II) as the metal ion as it usually displays diverse coordinating characteristics arising from Jahn–Teller distortion as well as the catalytic potential through coordinatively unsaturated copper sites.^[37,38] By inserting auxiliary ligands such as amines, new structural motives could be obtained as seen in the work of Mao et al.^[26–30] In order to gain insight into these structural possibilities, HT-screening of various solvents and copper(II) salts with an auxiliary diamine ligand, namely 4,4'-bipyridine (4,4'-*bipy*) was performed. This systematic investigation has resulted in the discovery and the synthesis optimization of a new mixed-ligand coordination polymer. Here, we report the synthesis, structural and magnetic characterization of a new copper(II)-coordination polymer containing H_3L and 4,4'-*bipy*, $[\text{Cu}(\text{HL})(4,4'\text{-bipy})]\cdot\text{H}_2\text{O}$ (**1**) and its structural conversion to the dehydrated compound $[\text{Cu}(\text{HL})(4,4'\text{-bipy})]$ (**1-h**).

Results and Discussion

HT-Screening of Solvents

Solubility of each reactant in the respective solvent plays an essential role in determining the outcome of a synthesis.^[39] Nonetheless, most metal phosphonates or sulfonates are synthesized in aqueous solution. In order to see the effects of other solvents on the synthesis, acetonitrile, 2-propanol and *N,N*-dimethylformamide (DMF) were also screened with $\text{Cu}(\text{NO}_3)_2\cdot 3\text{H}_2\text{O}$, H_3L and 4,4'-*bipy* (Tab. S1). All screening reactions in this stage were performed at a reaction temperature of 130 °C. The molar ratios of $\text{Cu}^{2+}:\text{H}_3\text{L}:4,4'\text{-bipy}$ were varied in the range of 1 to 3 in 1.0 steps. According to the X-ray powder diffraction (XRPD) measurements, 2-propanol-based syntheses yielded various mixed-phase products most of which contained **1**. Due to strong overlap of the reflections the identification of the other products was not accomplished. DMF-based reactions generated mixed phases mostly comprised of **1**, elemental copper, Cu_2O and $[\text{Cu}(4,4'\text{-bipy})(\text{OH})]$,^[40] which indicates that DMF can also act as a reducing agent under certain conditions.^[41] Acetonitrile-based reactions produced mixed phases in which green crystals were obtained. These were determined by XRPD measurements to be the known compound $[\text{Cu}_2(\text{CH}_3\text{COO})_4(4,4'\text{-bipy})]\cdot\text{CH}_3\text{CN}$.^[42] The acetate ion resulted from the in situ hydrolysis of acetonitrile. In general, the organic solvents are advantageous to increase the solubility of some amine ligands. Nevertheless, the usage of organic solvent is disadvantageous for our purposes as no new mixed-ligand coordination polymer was obtained. Only with water based synthesis led unequivocally to a new mixed-ligand compound, $[\text{Cu}(\text{HL})(4,4'\text{-bipy})]\cdot\text{H}_2\text{O}$ (**1**).

HT-Screening of Copper(II) Salts

The counterions of the copper salts affect the pH of the reaction mixture and can also induce in situ side-reactions such as

oxidation during the synthesis.^[18] In addition, the deployment of the suitable copper(II) salt could also prevent the co-crystallization of unwanted phases.^[36] In a HT-screening experiment with 24 individual reactions, other copper salts in addition to $\text{Cu}(\text{NO}_3)_2\cdot 3\text{H}_2\text{O}$ were tested with 4,4'-*bipy* under hydrothermal conditions (Tab. S2). The reaction involving $\text{CuCl}_2\cdot 2\text{H}_2\text{O}$ only yielded $\alpha\text{-}[\text{Cu}(4,4'\text{-bipy})\text{Cl}_2]$ which was identified via XRPD and elemental analysis.^[43] $\text{Cu}(\text{CH}_3\text{COO})_2\cdot\text{H}_2\text{O}$ always generated mixed phases of **1** with unidentified crystalline impurities and traces of Cu_2O . The use of $\text{CuSO}_4\cdot 5\text{H}_2\text{O}$ resulted only in mixtures of **1** with a small amount of crystalline impurities. The most suitable copper salt was determined to be $\text{Cu}(\text{NO}_3)_2\cdot 3\text{H}_2\text{O}$ since it resulted mostly in the pure phase **1** depending on the molar composition of the reaction mixtures. Looking closely at the various $\text{Cu}(\text{NO}_3)_2\cdot 3\text{H}_2\text{O}/\text{H}_3\text{L}/4,4'\text{-bipy}$ molar ratios used, the optimal reactant composition was determined to be 1:1:1. This molar ratio was successfully used for the synthesis scale up in glass tubes (see Exp. Sect.).

Crystal Structure

The asymmetric unit of **1** is comprised of two Cu^{2+} ions, one doubly deprotonated $(\text{HL})^{2-}$ ion, two 4,4'-*bipy* and a single water molecule (Figure 1).

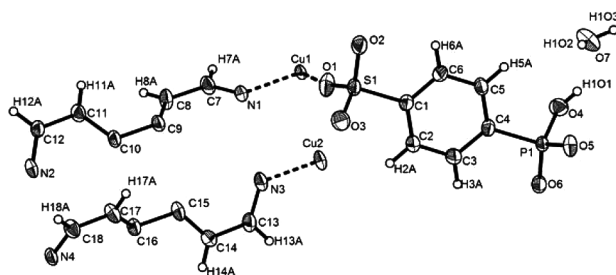


Figure 1. The asymmetric unit of compound **1**. The coordinative Cu–N and Cu–O bonds are depicted by broken lines. Thermal ellipsoids are drawn at 50 % probability.

The X-ray scattering factors of phosphorus and sulfur are very similar. Nevertheless, the distinction can be made by comparison of the P–O and S–O bond lengths. The P–O bond lengths of 1.489(2)–1.571(2) Å in **1** are longer than the S–O bonds, which are between 1.438(2) and 1.456(3) Å. These observations agree well with the values in the literature and facilitate the assignment of sulfur and phosphorus atoms.^[19,36,44]

The Cu^{2+} ions are surrounded by four oxygen atoms of the sulfonate and phosphonate ions as well as two nitrogen atoms of the 4,4'-*bipy* molecules to form a distorted CuN_2O_4 octahedra. The oxygen atoms of phosphonate ions and the nitrogen atoms lie on the equatorial positions in the octahedra whereas the oxygen atoms from the sulfonate ions are in the axial positions. The typical Jahn–Teller distortion can be observed with the elongated Cu–O axial bonds in the 2.556(2)–2.620(3) Å range (Figure 2A). The equatorial Cu–O and Cu–N bonds are in the range of 1.930(2)–1.942(2) Å and 2.008(3)–2.025(3) Å, respectively. These octahedra are interconnected via sulfur and

phosphorus atoms along the *c*-axis to form infinite chains (Figure 2A). The chains are cross-linked along the *b*-axis through 4,4'-*bipy* molecules and also through (HL)²⁻ ions in the (101) plane (Figure 3). A three-dimensional structure is thus formed. Weak hydrogen bonds ($D\cdots A = 2.614(3)$ – $2.819(3)$ Å) are observed between the water molecule and the oxygen atoms from the phosphonate and sulfonate ions (Figure 2A). The water molecules act twice as H-donor and once as H-acceptor.

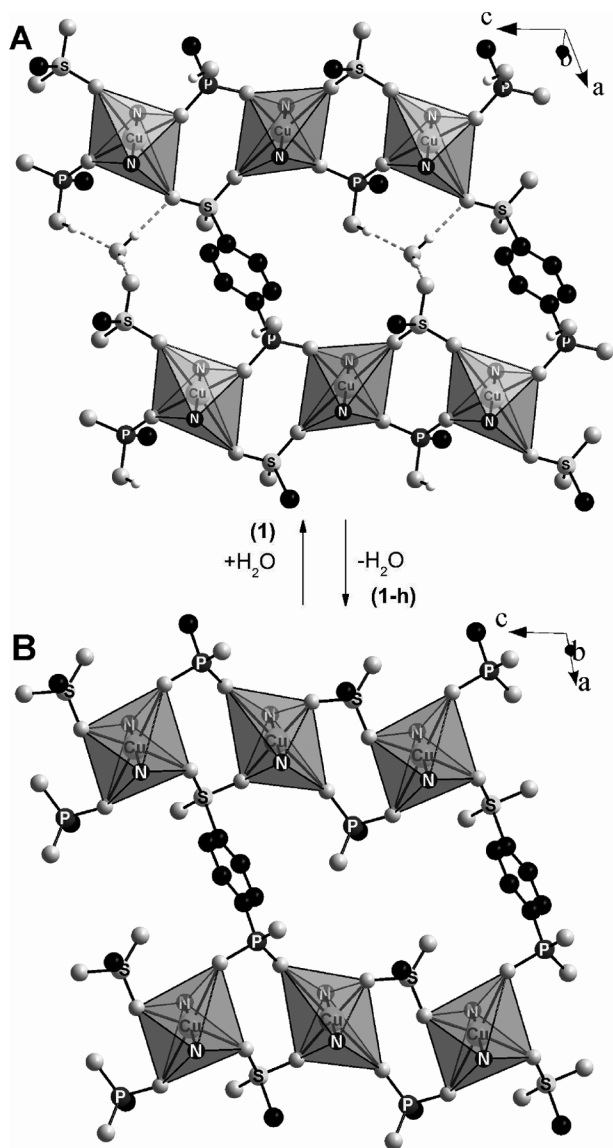


Figure 2. The chain-like interconnection of the CuN₂O₄ Jahn–Teller distorted octahedra by the sulfonate and phosphonate groups along the *c*-axis for the compound **1** (A) and **1-h** (B). The chains are linked to each other via the phenyl rings of the (HL)²⁻ ions. The elongated Cu–O axial bonds in **1** originate from sulfonate groups (A). In **1-h**, the elongation of Cu–O axial bonds involves the oxygen atoms of the phosphonate groups (B). Hydrogen atoms from the aromatic groups were omitted for clarity.

Thermal treatment at 250 °C leads to the removal of the H₂O molecules (see Thermal investigations). Changes in the unit cell parameters were observed with no symmetry changes. The

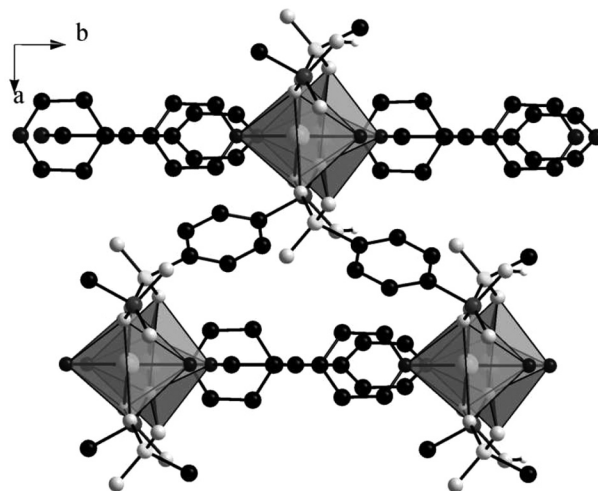


Figure 3. View along [001] showing the linkage of the chains of CuN₂O₄ octahedra to each other by the phenyl rings of (HL)²⁻ ions, and by the 4,4'-*bipy* ligands. The same arrangement is observed in both compounds **1** and **1-h**. Hydrogen atoms from the aromatic groups were omitted for clarity.

most apparent changes are a longer cell parameter *a* (+7.8 %) and a shorter cell parameter *c* (–3.7 %). The cell parameter *b*, which is exactly the distance between the chains connected by the 4,4'-*bipy* ligands, does not change significantly (Figure 3).

Typically, structural phase transitions are due to temperature changes,^[45] but in compound **1**, the transition to **1-h** seems to be caused by the dehydration of the compound as the dehydrated phase **1-h** is stable at room temperature. By exposing **1-h** to moisture, the structure converts gradually to the crystal structure of **1**, which was confirmed by XRPD analysis (Figure S1).

A possible explanation for the lengthening of cell parameter *a* could be the lack of the hydrogen bonds from the water molecules in **1**. This produces a repulsion of the chains from each other and thus increasing the cell length along the *a*-axis.

Looking closer at the atomic arrangements in **1-h**, the elongated Cu–O axial bonds of the Jahn–Teller distorted CuN₂O₄ octahedra are no longer between the oxygen atoms of sulfonate groups, but instead between the oxygen atoms of the phosphonate groups (Figure 2A, Figure 2B). This is similar to a so-called “Jahn–Teller switching”, which has been reported with several copper(II) containing compounds. In a Jahn–Teller distorted Cu(D₂O)₆²⁺ octahedra in the deuterated Tutton salt, Cu(D₂O)₆(ND₄)₂(SO₄)₂, the elongated axial bonds flip to different pairs of water molecules compared to hydrogenous compound.^[46] A pressure dependent “switching” also occurs in this compound upon raising the pressure from 1 to 1.5 bar.^[47] The changes in the local coordination environment of Cu²⁺ ion between compounds **1** and **1-h** can be attributed to the lack of hydrogen bonding from water molecules. Nevertheless, the reasoning behind this observation cannot be solely dependent on the water molecules, but also on the influence of the remainder of the whole structure.

Magnetic Investigations

To investigate the magnetic properties of **1**, the temperature dependence of its susceptibility was investigated by applying a magnetic field of $H = 1$ T in the temperature range of 2–300 K. The Cu^{2+} ions are only found in isolated CuN_2O_4 polyhedra and are connected by phosphonate and sulfonate groups ($\text{Cu}\cdots\text{Cu} = 5.356(1)$ Å). Due to the long exchange pathway, weak magnetic interactions are expected. Looking at the χ^{-1} vs. T plot fitted using the Curie–Weiss law $\chi = C/(T-\theta_w)$, an almost linear curve is observed which confirms the Curie–Weiss paramagnetism (Figure 4, top). A Weiss constant of 10.2 K was determined which indicates weak ferro-/ferrimagnetic interactions. This result is also supported by the plot of $\chi \cdot T$ vs. T in Figure 4 (bottom) that shows the domination of weak ferro-/ferrimagnetic behavior from 300 K to 3.5 K. At 3.5 K, the interaction switches to antiferromagnetic (see inset in Figure 4, bottom). The average effective magnetic moment of $1.69(4) \mu_B$ calculated from the fitted data from 40–300 K compares well with the theoretical spin-only value of $1.73 \mu_B$ (Figure 4). Upon further cooling from 40 K to 2 K, the μ_{eff} value dips exponentially which indicates complex magnetic interactions.

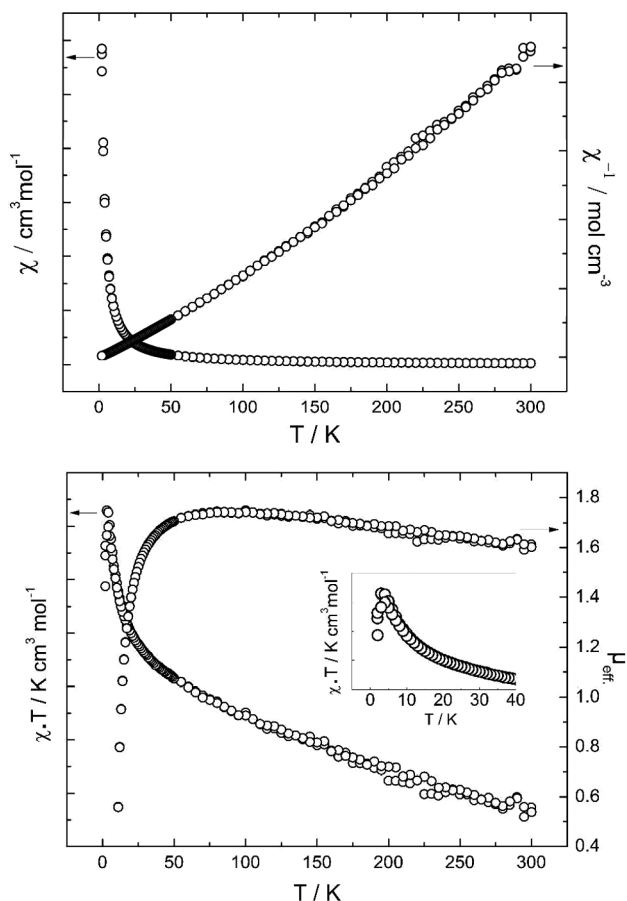


Figure 4. Results of the magnetic susceptibility measurements for **1**. Plots of paramagnetic and reciprocal paramagnetic susceptibility (top) as well as $\chi \cdot T$ and effective magnetic moment as function of temperature are shown. The inset graph displays the switching from ferro-/ferrimagnetic to antiferromagnetic interactions at 3.5 K.

Thermal Investigations

TG/DTA measurements have yielded much insight in the composition and the thermal stability of compound **1** (Figure S3). The solid product after the TG analysis was characterized by XRPD measurement. The endothermic dehydration of **1** is observed at 200 °C (weight loss % calcd./obs.: 3.9/4.1). The second weight loss stage (200–450 °C) is attributed to the loss of 4,4'-*bipy* molecules (% calcd./obs.: 32.9/32.0). The final step in the TG curve can be assigned to the disintegration of the $-\text{C}_6\text{H}_4-\text{SO}_3$ fragment of the $(\text{HL})^{2-}$ ions (% calcd./obs.: 33.0/32.1). The light blue colored solid residue was identified as $\text{Cu}_2\text{P}_2\text{O}_7$ by XRPD (% calcd./obs.: 31.8/31.7).

Temperature dependent XRPD measurements gave important evidence on the phase transition of **1** to **1-h** (Figure 5). Compound **1** is stable in the temperature range of 20–250 °C. Upon complete dehydration at 250 °C, **1-h** is formed, which decomposes at 340 °C. The obvious discrepancy in phase transition temperatures between TG (200 °C) and temperature dependent XRPD analyses (250 °C) is due to the difference in the sample setup (refer to Experimental Section).

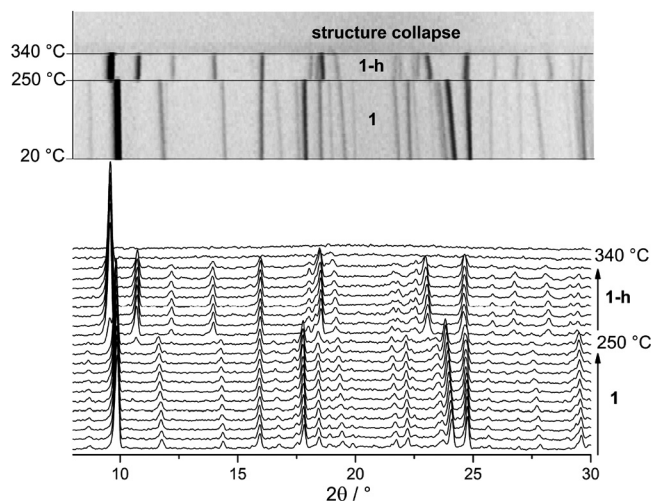


Figure 5. Results of the temperature-dependent XRPD investigation of a capillary tube sample shows the phase transition from **1** to **1-h** at 250 °C.

Conclusions

High-throughput methods have helped to identify and optimize the reaction conditions that led to the new mixed-linker coordination polymer $[\text{Cu}(\text{HL})(4,4'\text{-bipy})]\cdot\text{H}_2\text{O}$. Surprisingly the choice of Cu-salt and solvent has a strong influence on the structure formed. Thus, only the reaction in water led to a single-phase product of **1**. Although only very small pores are present in the structure of **1**, occluded water molecules can be reversibly removed. The often in coordination polymers observed structural flexibility leads in **1** to a substantial change in the coordination environment of the Jahn–Teller distorted CuN_2O_4 polyhedra. In **1** the elongated Cu–O axial bonds stem from the sulfonate groups whereas upon dehydration, they

originate from the phosphonate groups. Such switching phenomenon in the coordination environment of the Jahn–Teller distorted octahedra has been rarely observed in the literature.

Experimental Section

Materials and Characterization Methods: All chemicals were commercially available and used without further purification (Sigma–Aldrich and ABCR), except for 4-phosphonobenzene-sulfonic acid (H₃L) which was synthesized according to the procedure reported previously.^[48] The three step synthesis of H₃L was performed with 4-bromobenzenesulfonyl chloride as the starting reactant. High-throughput XRPD experiments were carried out in transmission mode using a STOE high-throughput powder diffractometer (Cu-*K*_{α1}, λ = 1.5406 Å) equipped with an image-plate position-sensitive detector (IPPSD). MIR spectra were recorded with an ATI Matheson Genesis spectrometer in the spectral range 4000–400 cm⁻¹ using the KBr disc method as well as an ALPHA-ST-IR Bruker spectrometer equipped with an ATR unit. Thermogravimetric analyses were carried out in air atmosphere (75 mL·min⁻¹, 30–800 °C, 4 °C·min⁻¹) using a NETZSCH STA 409 CD analyzer. The temperature dependent XRPD analysis in Debye–Scherrer mode was carried out on a STOE Stadi-P diffractometer (Cu-*K*_{α1}, λ = 1.5406 Å), equipped with a STOE high temperature capillary furnace, using 0.3 mm quartz capillary tubes. CHNS analyses were performed with an Eurovektor EuroEA Elemental Analyzer. The semi-quantitative elemental analyses were performed with a Phillips ESEM XL 30 hot cathode scanning electron microscope equipped with energy dispersive X-ray (EDX) EDAX analyzer for elemental analysis. Magnetic measurements for compound **1** was performed with a Physical Property Measuring System (PPMS) from Quantum Design (9 T magnet), at 1 T (DC field), respectively, in the temperature range of 2 to 300 K (ZFC). Diamagnetic susceptibility of compound **1** (–237.51 × 10⁻⁶ cm³·mol⁻¹) was calculated using the tables in the literature and diamagnetic correction was applied during the data analysis.^[49]

High-Throughput Experiments: The reaction system Cu²⁺/H₃L/4,4'-*bipy*/solvent was investigated using various molar ratios Cu²⁺/H₃L/4,4'-*bipy* employing high-throughput methods (process and compositional parameters are listed in Tab. S1–S2 in the Supporting Information). Each HT experiment was performed under solvothermal conditions in a custom-made stainless steel high-throughput reactor system containing 48 PTFE inserts each. The PTFE inserts have a maximum volume of 300 μL.^[34] All reagents were manually dosed using aqueous solutions of the reactants. The concentrations as well as the exact amounts of starting materials are given in the Table S1–S2. The evaluation of the HT experiments is based on XRPD measurements.

[Cu(HL)(4,4'-*bipy*)]·H₂O (1**):** In a typical HT experiment **1** was obtained by the following procedure (molar ratio Cu²⁺:H₃L:4,4'-*bipy* = 1:1:1). Aqueous solutions of Cu(NO₃)₂·3H₂O (0.02 mmol, 40 μL), H₃L (0.02 mmol, 20 μL), 4,4'-*bipy* (0.02 mmol, 20 μL) and additional H₂O (120 μL) were mixed in a 300 μL reactor and heated for 48 h at 130 °C. The scale-up of **1** was accomplished using glass tubes (DURAN® culture tubes 12 × 100 mm D50 GL 14 M.KAP, SCHOTT 261351155). Cu(NO₃)₂·3H₂O (500 μL, 0.2 mmol), H₃L (500 μL, 0.2 mmol), and 4,4'-*bipy* (1000 μL, 0.2 mmol) were combined and sonicated for 10 min. The mixture was heated at 130 °C for 48 h. The synthesis yielded a light blue powder (40 mg, 42 mol-% based on H₃L, final pH value of reaction mixture = 1–2) which was identified by XRPD. C₁₆H₁₅CuN₂O₇PS (molecular mass: 473.87 g/mol); C 40.6 (calcd. 40.5); H 2.9 (3.2); N 6.2 (6.0); S 6.8 (6.8)%. IR (KBr): $\tilde{\nu}$ =

(OH) 3410 cm⁻¹, ν (Ar-H) 3080 w, δ (OH) 1650 m, ν (C=C) 1600 m, ν (C=N) 1410 m, ν_{asym} (P–O, S–O) 1190 s, ν_{sym} (P–O, S–O) 1090 m, δ (Ar-H) 810 m, 645 s.

[Cu(HL)(4,4'-*bipy*)] (1-h**):** **1-h** was obtained by activating compound **1** at 200 °C under vacuum for 12 h. To avoid rehydration of **1-h** to **1**, the dehydrated substance was stored in a vacuum desiccator with KOH and P₂O₅ as the desiccant. C₁₆H₁₃CuN₂O₆PS (molecular mass: 455.88 g/mol); C 42.0 (calcd. 42.2); H 3.1 (2.9); N 6.1 (6.1); S 6.8 (7.0)%. IR (ATR): ν (Ar-H) 3070 cm⁻¹ w, ν (C=C) 1610 m, ν (C=N) 1410 m, ν_{asym} (P–O, S–O) 1140 s, ν_{sym} (P–O, S–O) 1000 m, δ (Ar-H) 810 m, 642 s.

X-ray Crystallography: A suitable crystal of the compound was carefully selected from the HT experiments using a polarizing microscope. Single-crystal X-ray diffraction for **1** was performed with a STOE IPDS-1 diffractometer equipped with a fine-focus sealed tube (Mo-*K*_α radiation, λ = 0.71073 Å). For data reduction and absorption correction the programs XRED and XSHAPE were used.^[50] The single crystal structure was solved by direct methods and refined using the program package SHELXTL.^[51] Experimental data and results of the structure determination of **1** are given in Table 1.

Table 1. Crystallographic data and details on the structure determination from single crystal of [Cu(HL)(4,4'-*bipy*)]·H₂O (**1**) and from Rietveld refinement of [Cu(HL)(4,4'-*bipy*)] (**1-h**).

	1	1-h
formula	C ₁₆ H ₁₅ CuN ₂ O ₇ PS	C ₁₆ H ₁₃ CuN ₂ O ₆ PS
MW /g·mol ⁻¹	473.87	455.89
crystal system	monoclinic	monoclinic
space group	C2 (no. 5)	C2 (no. 5)
<i>a</i> /Å	15.7374(12)	16.9581(7)
<i>b</i> /Å	11.0896(6)	11.1033(3)
<i>c</i> /Å	10.6253(8)	10.2310(5)
β /°	108.243(6)	103.866(2)
<i>V</i> /Å ³	1761.14(22)	1870.27(10)
<i>Z</i>	4	4
$\rho_{\text{calcd.}}$ /g·cm ⁻³	1.787	1.572
<i>T</i> /K	293 (5)	583 (5)
μ /mm ⁻¹	1.495	–
min/max transm.	0.770 / 0.862	–
$\theta_{\text{min.}}$, $\theta_{\text{max.}}$ /°	2–29.2	4–40
meas. reflns.	16314	–
unique reflns.	4619	–
reflns. [<i>F</i> _o > 4 σ (<i>F</i> _o)]	4368	–
parameter	258	70
<i>R</i> -values	<i>R</i> _{int} = 0.038 <i>R</i> ₁ , <i>wR</i> ₂ [all data] = 0.036, 0.071 <i>R</i> ₁ , <i>wR</i> ₂ [<i>F</i> _o > 4 σ (<i>F</i> _o)] = 0.032, 0.069	<i>R</i> _{exp} = 0.023 <i>R</i> _{Bragg} = 0.008 <i>R</i> _p = 0.032 <i>R</i> _{wp} = 0.042 1.805
GoF	1.085	–
$\Delta\rho_{\text{max.}}$, $\Delta\rho_{\text{min.}}$ /e ⁻ ·Å ⁻³	0.43, –0.38	–

The crystal structure of **1-h** was determined on the basis of X-ray powder diffraction data. The XRPD pattern of a capillary-filled sample was recorded with a STOE Stadi-P powder diffractometer in Debye–Scherrer geometry using Ge(111) monochromated Cu-*K*_{α1} radiation. The details of XRPD measurements are as following; 2 θ range = 8–80°, step width = 0.01, data points = 4800, no. of observed reflections = 105, *T* = 583(5) K. EXPO2009 software with TREOR indexing algorithm was used to determine the cell parameters.^[52] The Rietveld refinement (Figure 6) was performed with the TOPAS package^[53] using the structure of **1** as the starting model. Preferred orientation of

the crystallites was described with a spherical harmonics function of 4th order. 32 atomic, 18 profile and 20 background parameters (Chebyshev) were refined. The relevant crystallographic data and further details of the data collection are summarized in Table 1.

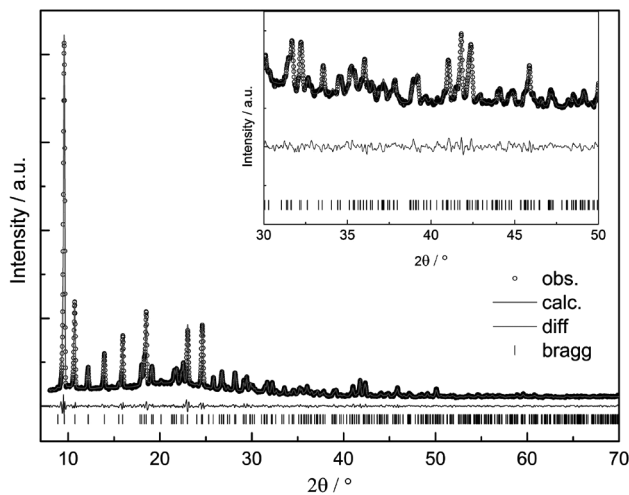


Figure 6. Observed (circles) and calculated (line) XRPD pattern as well as the difference profile of the Rietveld refinement of **1-h**; Allowed Bragg reflex positions are marked by vertical lines.

Crystallographic data (excluding structure factors) for the structures **1** and **1-h** reported in this paper have been deposited with the Cambridge Crystallographic Data Centre as supplementary publication no. CCDC-822923 (**1**) and -823351 (**1-h**). Copies of the data can be obtained free of charge on application to CCDC, 12 Union Road, Cambridge CB2 1EZ, UK [Fax: +44-1223-336-033; E-Mail: deposit@ccdc.cam.ac.uk].

Supporting Information (see footnote on the first page of this article): Experimental details of the HT-investigations; selected bond lengths and angles; comparison of measured and simulated XRPD patterns, IR spectroscopic data; TG / DTA analysis of **1**.

Acknowledgement

The authors thank *Inke Jeß* and Professor *Christian Näther* for the acquisition of the single-crystal data, *Beatrix Seidlhofer* for TG measurements, *Henning Lühmann* and *Maren Rassmussen* for magnetic measurements. This work was supported by the *Deutsche Forschungsgemeinschaft* (DFG) (STO 643/2).

References

- [1] C. Sanchez, B. Julian, P. Belleville, M. Popall, *J. Mater. Chem.* **2005**, *15*, 3559–3592.
- [2] A. Y. Robin, K. M. Fromm, *Coord. Chem. Rev.* **2006**, *250*, 2127–2157.
- [3] S. Kitagawa, R. Kitaura, S. Noro, *Angew. Chem.* **2004**, *116*, 2388–2430; *Angew. Chem. Int. Ed.* **2004**, *43*, 2334–2375.
- [4] H. Li, M. Eddaoudi, M. O’Keefe, O. M. Yaghi, *Nature* **1999**, *402*, 276–279.
- [5] A. Sonnauer, F. Hoffmann, M. Fröba, L. Kienle, V. Duppel, M. Thommes, C. Serre, G. Férey, N. Stock, *Angew. Chem.* **2009**, *121*, 3849–3852; *Angew. Chem. Int. Ed.* **2009**, *48*, 3791–3794.
- [6] D. N. Dybtsev, H. Chun, K. Kim, *Angew. Chem.* **2004**, *116*, 5143–5146; *Angew. Chem. Int. Ed.* **2004**, *43*, 5033–5036.

- [7] K. S. Park, Z. Ni, A. P. Cote, J. Y. Choi, R. Huang, F. J. Uribe-Romo, H. K. Chae, M. O’Keefe, O. M. Yaghi, *Proc. Natl. Acad. Sci. USA* **2006**, *103*, 10186–10191.
- [8] A. Clearfield, *Curr. Opin. Solid State Mater. Sci.* **2002**, *6*, 495–506.
- [9] D. K. Cao, S. Gao, L.-M. Zheng, *J. Solid State Chem.* **2004**, *177*, 2311–2315.
- [10] K. Maeda, *Microporous Mesoporous Mater.* **2004**, *73*, 47–55.
- [11] R.-G. Xiong, J. Zhang, Z.-F. Chen, X.-Z. You, C.-M. Che, H.-K. Fun, *J. Chem. Soc., Dalton Trans.* **2001**, 780–782.
- [12] G. K. H. Shimizu, R. Vaidyanathan, J. M. Taylor, *Chem. Soc. Rev.* **2009**, *38*, 1430–1449.
- [13] S. Natarajan, P. Mahata, *Curr. Opin. Solid State Mater. Sci.* **2009**, *13*, 46–53.
- [14] N. Stock, T. Bein, *J. Mater. Chem.* **2005**, *15*, 1384–1391.
- [15] C. Serre, N. Stock, T. Bein, G. Férey, *Inorg. Chem.* **2004**, *43*, 3159–3163.
- [16] N. Stock, A. Stoll, T. Bein, *Microporous Mesoporous Mater.* **2004**, *69*, 65–69.
- [17] S. Bauer, T. Bein, N. Stock, *J. Solid State Chem.* **2006**, *179*, 145–155.
- [18] S. Bauer, T. Bein, *Inorg. Chem.* **2005**, *44*, 5882–5899.
- [19] A. Sonnauer, N. Stock, *Eur. J. Inorg. Chem.* **2008**, 5038–5045.
- [20] A. Sonnauer, M. Feyand, N. Stock, *Cryst. Growth Des.* **2009**, *9*, 586–592.
- [21] A. Sonnauer, N. Stock, *Solid State Sci.* **2009**, *11*, 358–363.
- [22] A. Sonnauer, N. Stock, *J. Solid State Chem.* **2008**, *181*, 473–479.
- [23] A. Sonnauer, C. Näther, H. A. Hoppe, J. Senker, N. Stock, *Inorg. Chem.* **2007**, *46*, 9968–9974.
- [24] A. Sonnauer, N. Stock, *J. Solid State Chem.* **2008**, *181*, 3065–3070.
- [25] M. Feyand, C. Näther, A. Rothkirch, N. Stock, *Inorg. Chem.* **2010**, *49*, 11158–11163.
- [26] Z.-Y. Du, H.-B. Xu, J.-G. Mao, *Inorg. Chem.* **2006**, *45*, 9780–9788.
- [27] Z.-Y. Du, H.-B. Xu, J.-G. Mao, *Inorg. Chem.* **2006**, *45*, 6424–6430.
- [28] Z.-Y. Du, V. A. Prosvirin, J.-G. Mao, *Inorg. Chem.* **2007**, *46*, 9884–9894.
- [29] Z.-Y. Du, X.-L. Li, Q.-Y. Liu, J.-G. Mao, *Cryst. Growth Des.* **2007**, *7*, 1501–1507.
- [30] Z.-Y. Du, H.-B. Xu, X.-L. Li, J.-G. Mao, *Eur. J. Inorg. Chem.* **2007**, 4520–4529.
- [31] F. Adani, M. Casciola, D. J. Jones, L. Massinelli, E. Montoneri, J. Rozière, R. Viviani, *J. Mater. Chem.* **1998**, *8*, 961–964.
- [32] A. F. Benedetto, P. J. Squattrito, F. Adani, E. Montoneri, *Inorg. Chim. Acta* **1997**, *260*, 207–216.
- [33] N. Stock, T. Bein, *Angew. Chem.* **2004**, *116*, 767–770; *Angew. Chem. Int. Ed.* **2004**, *43*, 749–752.
- [34] N. Stock, *Microporous Mesoporous Mater.* **2010**, *129*, 287–295.
- [35] S. Bauer, N. Stock, *Angew. Chem.* **2007**, *119*, 6981–6984; *Angew. Chem. Int. Ed.* **2007**, *46*, 6857–6860.
- [36] P. Maniam, C. Näther, N. Stock, *Eur. J. Inorg. Chem.* **2010**, 3866–3874.
- [37] H. A. Jahn, E. Teller, *Proc. R. Soc. London Ser. A* **1937**, *161*, 220–235.
- [38] L. Alaerts, E. Séguin, H. Poelman, F. Thibault-Starzyk, P. A. Jacobs, D. E. De Vos, *Chem. Eur. J.* **2006**, *12*, 7353–7363.
- [39] J. Fan, M. H. Shu, T. Okamura, Y. Z. Li, W. Y. Sun, W. X. Tang, N. Ueyama, *New J. Chem.* **2003**, *27*, 1307–1309.
- [40] S. P. Chen, G. Fan, S. L. Gao, *Acta Chim. Sinica* **2007**, *65*, 1385–1388.
- [41] I. Pastoriza-Santos, L. M. Liz-Marzán, *Pure Appl. Chem.* **2000**, *72*, 83–90.
- [42] Y. H. Wen, Y. H. He, Y. L. Feng, *Chin. J. Struct. Chem.* **2007**, *26*, 29–32.
- [43] N. Masciocchi, P. Cairati, L. Carlucci, G. Mezza, G. Ciani, A. Sironi, *J. Chem. Soc., Dalton Trans.* **1996**, 2739–2746.
- [44] P. Maniam, N. Stock, *Acta Crystallogr., Sect. C* **2011**, *67*, m73–m76.

- [45] Y. Liu, J. H. Her, A. Dailly, A. J. Ramirez-Cuesta, D. A. Neumann, C. M. Brown, *J. Am. Chem. Soc.* **2008**, *130*, 11813–11818.
- [46] B. J. Hathaway, A. W. Hewat, *J. Solid State Chem.* **1984**, *51*, 364–375.
- [47] C. J. Simmons, M. A. Hitchman, H. Stratemeier, A. J. Schultz, *J. Am. Chem. Soc.* **1993**, *115*, 11304–11311.
- [48] E. Montoneri, G. Viscardi, S. Bottigliengo, R. Gobetto, M. R. Chierotti, R. Buscaino, P. Quagliotto, *Chem. Mater.* **2007**, *19*, 2671–2678.
- [49] G. A. Bain, J. F. Berry, *J. Chem. Educ.* **2008**, *85*, 532–536.
- [50] *XRED version 1.19, XSHAPE version 1.06*, Stoe & Cie GmbH, Darmstadt, Germany, **1999**.
- [51] G. M. Sheldrick, *Acta Crystallogr., Sect. A* **2008**, *64*, 112–122.
- [52] A. Altomare, M. Camalli, C. Cuocci, C. Giacovazzo, A. Moliterni, R. Rizzi, *J. Appl. Crystallogr.* **2009**, *42*, 1197–1202.
- [53] A. A. Coelho, *TOPAS-Academic v4.1*; Coelho Software, Brisbane, **2007**.

Received: May 1, 2011
Published Online: June 14, 2011